Green Intelligent Systems and Applications

Research Article
Volume 5(2), 2025, 164−180
https://doi.org/10.53623/gisa.v5i2.880

Temporal Analysis of Land Subsidence in DKI Jakarta Using the Long Short-Term Memory (LSTM) Model

Heni Fitriany[1], Panca Dewi Pamungkasari[1]*, Yunan Fauzi Wijaya[1], Muhammad Fauzan Azhiman[1], Yasuhito Nagase[2], Joko Widodo[3]

[1]Universitas Nasional Faculty of Communication and Information Technology, Jakarta, Indonesia
[2]Department of Earth and Environmental Sciences, Graduate School of Science and Engineering, Chiba University, Chiba, Japan
[3]Research and Innovation Agency (BRIN), Jakarta 10340, Indonesia

*Correspondence: panca.dewi79@gmail.com

SUBMITTED: 6 November 2025; REVISED: 6 December 2025; ACCEPTED: 10 December 2025

ABSTRACT: This research investigated temporal patterns of land subsidence in DKI Jakarta by applying a Long Short-Term Memory (LSTM) model to deformation measurements derived from Persistent Scatterer Interferometric Synthetic Aperture Radar (PS-InSAR) observations acquired between 2017 and 2021. Because the original PS-InSAR time series was characterized by uneven acquisition intervals, the deformation records were first resampled into a uniform 11-day sequence to obtain a consistent temporal structure for modeling. Preprocessing steps, comprising outlier handling, temporal resampling, and feature normalization, were performed to ensure that the model could capture deformation behavior reliably. The LSTM architecture employed three stacked recurrent layers and was trained using the Adam optimizer with Smooth L1 Loss and an early-stopping strategy. Model evaluation demonstrated excellent agreement between predicted and observed deformation, yielding R^2 = 1.000, MSE = 0.104, RMSE = 0.322 mm, and KGE = 0.998. Compared with a previously developed Random Forest model (R^2 = 0.9995, RMSE = 0.3314 mm), the LSTM approach exhibited more stable temporal learning and was better suited for long-horizon deformation forecasting. Spatial analysis revealed that northern Jakarta, particularly Cengkareng, Tanjung Priok, and Pantai Indah Kapuk, continued to experience the greatest cumulative subsidence (> −30 mm), whereas areas in the south, such as Jagakarsa and Kebayoran Baru, showed minimal deformation (< −5 mm), aligning with known geological and anthropogenic conditions. Overall, integrating PS-InSAR time series with an LSTM framework provided a more coherent and temporally consistent method for characterizing subsidence behavior in Jakarta. The outcomes of this study offered a scientific basis for developing intelligent monitoring tools to support mitigation efforts and sustainable urban planning in regions affected by land subsidence.

KEYWORDS: Land subsidence; Jakarta; PS-InSAR; LSTM; deep learning; temporal prediction

1. Introduction

Land subsidence is one of the most serious geotechnical hazards faced by many major cities worldwide, particularly in Asian regions experiencing rapid urbanization and excessive groundwater extraction [1, 2]. This phenomenon is defined as a gradual decrease in ground surface elevation caused by natural sediment compaction and anthropogenic activities such as deep groundwater pumping and heavy building loads [3]. In Indonesia, land subsidence has become a major environmental issue in several large cities, including Jakarta, Bandung, and Semarang, resulting in infrastructure damage, increased frequency of tidal flooding, and seawater intrusion into inland areas [4]. According to Abidin et al., land subsidence in Jakarta has occurred for more than four decades, with rates reaching 3–10 cm per year, particularly in northern coastal areas such as Cengkareng, Penjaringan, and Tanjung Priok. The main factors driving subsidence are deep groundwater extraction and the presence of young alluvial sediments, which have caused tilted buildings, road cracking, and reduced drainage effectiveness. Research by Sarah [2] and Bott et al. [1] indicated that more than 70% of urban land subsidence in Indonesia is anthropogenic, although most communities remain unaware that it is the main cause of increasing tidal flooding.

The development of remote sensing technology based on Interferometric Synthetic Aperture Radar (InSAR) has enabled accurate spatial and temporal mapping of land deformation. Sidiq et al. [4] utilized Sentinel-1 SAR data from 2017–2023 to identify deformation rates ranging from 60–200 mm/year across major cities in Java Island. Widodo et al. [5] analyzed land subsidence in DKI Jakarta using the Persistent Scatterer Interferometric Synthetic Aperture Radar (PS-InSAR) method with TerraSAR-X data from 2017–2021, showing that Pantai Indah Kapuk and Kembangan experienced significant cumulative subsidence of approximately 9.85 cm and 5.63 cm, respectively, primarily due to excessive groundwater extraction and alluvial sediment compaction. These studies demonstrated the effectiveness of PS-InSAR for monitoring temporal and spatial ground deformation in densely populated urban areas.

Several studies have applied machine learning to model and predict land subsidence based on InSAR data. Hakim et al. [6] developed a Functional and Meta-Ensemble Machine Learning model (RF, GBT, and SVM) with an AUC of 0.94; however, the model was spatially static and did not represent temporal dynamics. Hidayah et al. [7] employed the Random Forest algorithm for temporal prediction, but the perfect accuracy ($R^2 = 1.000$) suggested temporal data leakage caused by random splitting without considering chronological order, allowing the model to indirectly access future data during training and producing unrealistically high performance.

To overcome these limitations, deep learning approaches have been developed for time-series-based ground deformation analysis. Li et al. [8] applied Long Short-Term Memory (LSTM) models to predict land subsidence in the Beijing Plain using InSAR and hydrogeological data from 2011–2015, achieving an RMSE of 14.41 mm and effectively capturing nonlinear relationships and long-term temporal patterns. Liu and Zhang [9] integrated SBAS-InSAR with an Attention-based LSTM (AT-LSTM) in the Pingshuo mining area, China (2019–2022), obtaining correlation >0.97 and MAE of 0.73 mm, demonstrating that attention mechanisms improved prediction accuracy and stability. More recently, Soni et

al. [12] showed that improved LSTM architectures further enhanced accuracy and stability, achieving RMSE below 5 mm/year in mining-induced subsidence studies.

Although LSTM and its derivatives have proven effective for modeling temporal dynamics of land subsidence, their application in highly anthropogenic urban areas such as DKI Jakarta remains limited. This study builds upon Hidayah et al. [7] by addressing the data leakage problem through chronological dataset splitting and implementing automatic temporal interpolation every 11 days to produce consistent, fixed-frequency data. This approach allows the LSTM model to realistically learn ground deformation patterns without temporal information leakage, resulting in more stable and replicable predictions. Additionally, fixed-interval temporal regularization was introduced to eliminate long observational gaps and produce a continuous deformation time series suitable for deep temporal learning. These refinements enable the model to learn smoother deformation trajectories and avoid unrealistic fluctuations, representing a substantial improvement in modeling accuracy and temporal stability compared to previous approaches.

This study also addresses challenges posed by highly heterogeneous and anthropogenically driven deformation patterns in megacities such as Jakarta. While prior work focused on mining regions or hydrogeologically uniform plains, the present study demonstrates that LSTM remains stable and predictive even under complex urban conditions characterized by strong spatial variability, multiple triggering mechanisms, and dense built-up areas. Furthermore, the research leverages a larger PS-InSAR dataset in both spatial density and temporal coverage than most prior deep learning studies, enabling more reliable modeling of long-term deformation behavior.

In the broader context of Green Intelligent Systems, accurate and continuous subsidence prediction supports environmentally sustainable urban management. Time-series forecasting enables intelligent monitoring systems to detect early signs of land instability, optimize groundwater extraction policies, and guide adaptive infrastructure planning in sinking coastal regions. By integrating PS-InSAR observations with deep learning-based temporal modeling, this research contributes to data-driven decision-support systems that enhance climate resilience, reduce disaster risk, and promote sustainable land and water resource governance in rapidly urbanizing megacities such as Jakarta. Consequently, this study provides a more reliable computational approach for temporal analysis of land subsidence in DKI Jakarta, serving as a scientific foundation for subsidence risk mitigation and urban groundwater management.

2. Materials and Methods

In general, the stages of this research include the preprocessing of PS-InSAR data, temporal interpolation, data normalization, LSTM model training, and result evaluation. The overall methodological workflow is illustrated in Figure 1 below.

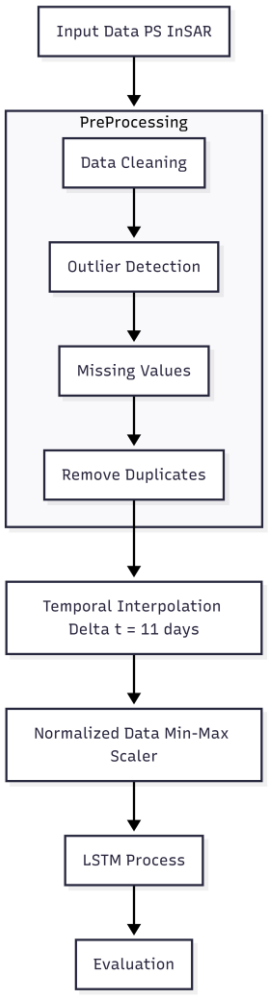

Figure 1. Research methodology workflow.

2.1. Dataset.

The dataset used in this study was generated from ground deformation processing using the Persistent Scatterer Interferometric Synthetic Aperture Radar (PS-InSAR) method developed by Widodo et al. [5]. TerraSAR-X images acquired between 20 October 2017 and 12 June 2021 were processed using SARPROZ software (version 7.3), producing deformation measurements at approximately 91,000 stable points distributed across all administrative regions of DKI Jakarta.

PS-InSAR is a multitemporal radar interferometry technique that tracks phase changes in radar returns from long-lasting reflective objects, such as buildings, paved surfaces, and other urban structures, to estimate ground motion with millimeter-level precision. Because these objects remain stable over time, they act as persistent scatterers, enabling continuous monitoring of subtle elevation changes.

The dataset included several key parameters: geographic coordinates (LAT, LON), elevations (HEIGHT and HEIGHT WRT DEM), average deformation velocity (VEL) and its standard deviation (SIGMA VEL), cumulative deformation (CUMUL.DISP.), and coherence (COHER). Together, these variables revealed spatial patterns of land subsidence across Jakarta. Consistent with previous studies, the largest subsidence occurred in the northern and western coastal districts, such as Penjaringan, Cengkareng, and Kalideres, whereas the southern part of the city remained comparatively stable.

Two versions of the time-series data were used in this research. The first consisted of the original PS-InSAR output, which contained irregular temporal intervals similar to those analyzed by Hidayah et al. [7]. The second was a temporally regularized version developed in this study, in which the deformation series was interpolated to a uniform 11-day interval. This interpolation aligned the data with the nominal revisit time of Sentinel-1A in equatorial regions and minimized the effects of long observational gaps (up to 88 days). Comparing the two datasets allowed us to assess how temporal irregularity influenced the performance and stability of the LSTM prediction model.

2.2. Pre-Processing Dataset.

The preprocessing stage was conducted to ensure that the PS-InSAR dataset was clean, consistent, and suitable for temporal interpolation and LSTM training. The process included duplicate checking, outlier reduction, handling of missing temporal values, and preparation of the data for the resampling stage.

2.2.1. Data Duplication Checking and Removal.

An initial check confirmed that no duplicate rows existed in the dataset. However, several temporal fields with the suffix ".1" (e.g., 20171020_HH and 20171020_HH.1) appeared as duplicated columns generated during SARPROZ export. These columns contained identical deformation values and were removed to avoid redundancy. After this step, 45 valid fields and 91,987 unique observation points remained.

2.2.2. Outlier Detection and Treatment.

To improve numerical stability, mild outliers in static attributes (HEIGHT, VEL, CUMUL.DISP., COHER, etc.) were filtered using interquartile range (IQR)-based trimming, whereas extreme temporal spikes were reduced using a Z-score threshold. Instead of deleting records, outlier values were replaced with the median of each field to preserve spatial coverage.

2.2.3. Handling Missing Values

Some deformation dates contained missing values due to radar acquisition gaps or low coherence. These gaps were filled using linear interpolation along the temporal axis so that each point retained a continuous time series prior to the resampling stage.

2.2.4. Temporal Interpolation

PS-InSAR acquisition dates are irregular and contain long temporal gaps (11–88 days). Such uneven sampling may introduce biases in temporal learning for sequence models. To address this problem, the cleaned deformation series were resampled to a fixed 11-day interval, corresponding to the nominal revisit time of Sentinel-1A in equatorial regions.

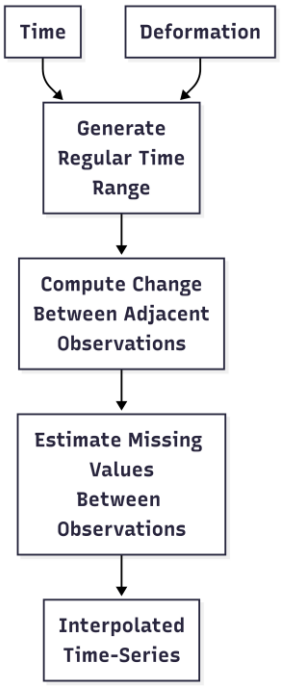

Figure 2. Workflow diagram of the PS-InSAR temporal interpolation process.

After cleaning and preparing the temporal fields, the deformation dates were converted into a complete 11-day calendar, and missing timestamps were filled using linear interpolation. This transformation produced a uniform set of 122 observations from the original 29 acquisition dates. The regularised dataset provides a more stable temporal input for the LSTM model and removes the long temporal gaps that affected the Random Forest approach in Hidayah et al. [7]. A summary of the resampling steps is presented in Table 1, and the mathematical interpolation formulation is shown in Equation (1). These details are provided to clarify the temporal regularisation process while keeping the main description concise.

Table 1. Step-by-step application algorithm of PS-InSAR temporal interpolation.

Algorithm 1 — Temporal Interpolation (11-day interval)

Input: PS-InSAR time-series with irregular sampling
Result: Regularized displacement time-series (Δt = 11 days)

```
df_all ← copy(df)
info_cols ← ['ID', 'LAT', 'LON', 'HEIGHT', 'HEIGHT WRT DEM',
             'SIGMA HEIGHT', 'VEL', 'SIGMA VEL', 'SEASONAL',
             'CUMUL.DISP.', 'COHER', 'SVET', 'LVET', 'IN', 'FIN',
date_cols_df ← df_all.drop(columns = info_cols)
info_df ← df_all[info_cols].set_index('ID') date_cols_df.columns ←
to_datetime(date_cols_df.columns.str.replace('_HH', ''),
                              format = '%Y%m%d', errors = 'coerce')
full_date_range ← date_range(start = min(date_cols_df.columns),
                         end   = max(date_cols_df.columns),
                         freq  = '11D')
reindexed_df ← date_cols_df.reindex(columns = full_date_range)
interpolated_dates ← reindexed_df.interpolate(method = 'linear', axis =
1)
final_df ← concat([info_df, interpolated_dates], axis = 1)
df ← copy(final_df)
return final_df
```

For missing timestamps, linear interpolation was applied along the temporal axis using the formula:

$$D(t_i) = D(t_{i-1}) + \frac{D(t_{i+1}) - D(t_{i-1})}{t_{i+1} - t_{i-1}} \times (t_i - t_{i-1}) \quad (1)$$

This equation estimates the deformation value at time t_i under the assumption that displacement evolves linearly between adjacent valid observations.

The selection of linear interpolation was based on its documented suitability for InSAR deformation time-series, where ground motion typically evolves gradually and exhibits quasi-linear behaviour over short temporal intervals. Linear interpolation avoids the oscillatory artefacts that may arise from higher-order methods such as spline interpolation, which can artificially amplify deformation signals between observation dates. In contrast, Kalman filtering and other state-space estimators require explicit dynamical models or noise parameters that are often unavailable for PS-InSAR deformation, especially in heterogeneous urban environments. Machine-learning-based temporal gap filling methods were not adopted because they require additional training labels and may introduce model-dependent biases. Several recent studies have also applied linear interpolation for temporal regularisation of InSAR time series due to its stability, simplicity, and ability to preserve large-scale deformation trends without overfitting [8] [12]. For these reasons, linear interpolation provides a balanced and physically consistent approach for reconstructing missing PS-InSAR observations in this study.

In addition to the interpolation procedure, it is important to evaluate how the temporal restructuring changes the characteristics of the PS-InSAR dataset. The resampling process not only increases the number of deformation timestamps but also alters the temporal density, continuity, and suitability of the data for sequence-based learning. By examining these structural differences, we can better understand why the regularised dataset produces more stable behaviour in the LSTM model compared with the irregular time series used in the earlier study. Moreover, understanding these temporal differences is essential because they directly influence how the model interprets long-term deformation trends and how stable its predictions become under different sampling conditions. A summary of these differences is presented in Table 2.

Table 2. Comparison between the dataset of Hidayah et al. [7] vs and this study.

Parameter	Hidayah et al.	This Study
Data Period	20 Okt 2017 – 12 Jun 2021	20 Okt 2017 – 12 Jun 2021
Number of Dates	29 Dates	122 Dates
Temporal Interval	Irregular (11–88 days)	Regular (11 days)
Examples of Gaos	14 Apr 2018 – 11 Jul 2018 (87 days) 12 Des 2018 – 10 Mar 2019 (88 days)	None
Temporal Consistency	Not Continuous	Continuous and regular
Model	Random Forest	LSTM

2.3. Model Long Short-Term Memory (LSTM).

The LSTM architecture was employed to model temporal patterns of ground deformation extracted from the regularised PS-InSAR time series. LSTM networks belong to the Recurrent Neural Network (RNN) family and are specifically designed to capture long-term dependencies through memory cells and gated operations. This capability makes LSTM suitable for representing gradual subsidence trends and nonlinear temporal behaviour. The input sequences were generated using a sliding-window approach, where 12 consecutive deformation values (132 days) were used to predict the next observation. Each window also included an auxiliary Δt feature to preserve temporal spacing information. All features were standardised using the

mean and standard deviation computed from the training portion of the data. An 80–20 chronological split was used to prevent temporal leakage, ensuring that future dates were never included during model training.

The model consisted of three LSTM layers with 256 hidden units per layer, followed by a fully connected output layer that produced a single displacement prediction. Dropout (0.3) was applied between layers for regularisation. The network was trained using the Adam optimiser with a learning rate of 5×10^{-4} and Smooth L1 Loss for robustness against outliers. Training was conducted for up to 80 epochs with early stopping based on validation loss. A ReduceLROnPlateau scheduler was used to reduce the learning rate when improvement stagnated. A high-level summary of the training workflow including window generation, normalisation, forward propagation, validation, and checkpointing is presented in Algorithm 3.

Table 3. Step-by-step algorithm of LSTM model training.

Algorithm 2 — LSTM Model Training Procedure

Input: Regularized PS-InSAR time-series dataset (Δt = 11 days)
Result: Trained LSTM model for displacement prediction
seed ← 42
device ← "cuda" if available else "cpu"
X_tr, y_tr, td_tr ← make_windows(df_ff, dates, seq_len=12, …)
X_te, y_te, td_te ← make_windows(df_ff, dates, seq_len=12, …)
μ, σ ← mean(X_tr), std(X_tr)
X_tr_n ← (X_tr – μ) / σ
y_tr_n ← (y_tr – μ_y) / σ_y
model ← LSTMRegressor(input_size=2, hidden_size=256, num_layers=3, dropout=0.3)
optimizer ← Adam(lr=5e-4, weight_decay=1e-5)
loss_fn ← SmoothL1Loss()
scheduler ← ReduceLROnPlateau(factor=0.5, patience=5)
for epoch in [1, …, 80] do:
    train_loss ← compute_loss(model, train_loader)
    val_loss ← compute_loss(model, test_loader)
    scheduler.step(val_loss)
    if val_loss < best_loss – δ: save_state(model)
    else: bad_epochs += 1
    if bad_epochs ≥ patience: stop_training()
save(model_state, "best_lstm_model.pth")

Before presenting the architectural specifications, it is important to summarise the key training components that define how the model learns temporal deformation patterns. These components include the number of layers, activation functions, optimiser settings, batch sizes, and early-stopping criteria, all of which influence training stability and convergence behaviour. The main architectural and optimisation parameters used in this study are listed in Table [4].

Table 4. LSTM model specifications and training parameters.

Component	Specification
Implementation Platform	PyTorch
Architecture	3 Hidden Layer + 1 Fully Connected Output Layer
Hidden Size	256 Neurons per Layer
Dropout	0.3
Activation Function	*tanh*
Loss Function	Smooth1Loss
Optimizer	Adam
Learning Rate	0.0005
Batch Size	128 (train), 512 (test)
Maximum Epoch	80
Early Stopping	Enable
Input Feature	Regularized temporal deformation values (11-day interval)
Ouput	Cumulative deformation (CUMUL.DISP.)

In addition to the main training configuration, a small exploratory hyperparameter tuning experiment was conducted to evaluate the sensitivity of the LSTM architecture to variations in hidden size, number of layers, dropout rate, and learning rate. These tuning trials were intentionally limited to short training runs (10 epochs) to identify parameter combinations that demonstrated stable behaviour and promising early-stage validation performance. This exploratory tuning served as supplementary analysis and did not replace the main architecture used in full training.

The exploratory results showed that several alternative configurations achieved lower validation loss during short-run evaluations. For example, a two-layer LSTM with 256 hidden units and a dropout rate of 0.2 produced the lowest validation loss among the tested models, while a three-layer architecture with 128 hidden units also performed competitively. These findings suggest that other architectures may also model deformation patterns effectively; however, because these experiments were conducted on short iterations, they do not reflect full convergence of the models.

Model performance in LSTM networks is sensitive to architectural choices such as hidden-size, depth, dropout, and learning rate. Therefore, a small exploratory hyperparameter search was conducted to compare multiple candidate configurations. Although a 128-unit, 3-layer model yielded slightly lower short-run validation loss, the 256-unit, 3-layer configuration was retained for full training because it demonstrated more stable convergence on the complete dataset. This decision aligns with prior research on InSAR-based deformation modelling, where deeper LSTM structures were found to be more robust to noise and long time series.

Other recurrent architectures such as GRU, bidirectional LSTM, and attention-based models were also considered during the model design phase; however, these alternatives were not implemented due to the substantial computational cost required to train them on the full PS-InSAR dataset, which contains more than 91,000 spatial points and 122 temporal observations. Prior studies have shown that the performance gains of these architectures are typically more pronounced when multi-source predictors (e.g., hydrological or environmental variables) are available, whereas the present study focuses on a univariate deformation time series. For this reason, the exploratory search was restricted to standard LSTM variants, which provided a strong balance between accuracy, model stability, and computational feasibility for large-scale deformation modelling.

2.4. Evalution.

The evaluation stage was conducted to assess the performance of the Long Short-Term Memory (LSTM) model in predicting ground surface deformation based on time-series data derived from PS-InSAR processing. This evaluation aimed to ensure that the model was not only capable of fitting the training data but also exhibited strong generalization ability when applied to new data (testing dataset). The evaluation process was carried out after the model had been fully trained and the best model checkpoint was obtained through the early stopping mechanism. Testing was performed by comparing the predicted deformation values against the actual observed values during the testing period (May 10 – June 12, 2021). To measure model performance, four primary statistical metrics were used: Root Mean Square Error (RMSE), Mean Absolute Error (MAE), Coefficient of Determination (R^2), and Kling–Gupta Efficiency (KGE). These four metrics were selected because, collectively, they provide a comprehensive

assessment of the model's accuracy, stability, and temporal pattern consistency in deformation prediction.

2.4.1. Root Mean Square Error (RMSE).

Root Mean Square Error (RMSE) is used to measure the average squared difference between the predicted and actual values. The smaller the RMSE value, the higher the model's accuracy. This metric is sensitive to large errors (outliers), making it effective for evaluating the precision of extreme deformation predictions.

$$RMSE = \sqrt{\frac{1}{n}\sum_{i=1}^{n}(y_i - \hat{y}_i)^2} \tag{2}$$

where y_i represents the actual deformation value and $\hat{y}_i$ denotes the model-predicted value. Recent studies highlight that RMSE remains an important metric in the evaluation of numerical models; however, it should be used in conjunction with other metrics, as the error distribution may influence the interpretation of results.

2.4.2. Mean Absolute Error (MAE).

Mean Absolute Error (MAE) represents the average magnitude of absolute errors between the predicted and observed values, regardless of the direction of deviation. A lower MAE value indicates that the model's predictions have a smaller average error.

$$MAE = \frac{1}{n}\sum_{i=1}^{n}|y_i - \hat{y}_i| \tag{3}$$

Unlike RMSE, MAE is not highly sensitive to extreme values, thus providing a more stable view of the model's overall performance.

*2.4.3. Coefficient of Determination (*R²*).*

The coefficient of determination (R^2) indicates the extent to which the model can explain the variability of the actual data. The R^2 value ranges from 0 to 1, where values closer to 1 indicate that the model can explain almost all variations in the observed data.

$$R^2 = 1 - \frac{\sum_{i=1}^{n}(y_i - \hat{y}_i)^2}{\sum_{i=1}^{n}(y_i - \bar{y})^2} \tag{4}$$

where $\bar{y}$ represents the mean value of the actual observations. A high R^2 value indicates that the model has strong predictive capability and a strong relationship with the observed data.

*2.4.3. Kling-Gupta Efficiency (*KGE*).*

The Kling–Gupta Efficiency (KGE) is used to evaluate the temporal pattern agreement between the predicted and observed results. In addition to considering the correlation coefficient (r), it also accounts for the mean bias and the variability ratio between datasets. This metric is particularly suitable for hydrological or land deformation modeling, as it effectively assesses the dynamic similarity of temporal patterns.

$$KGE = 1 - \sqrt{(r-1)^2 + (\frac{\sigma_x/\mu_x}{\sigma_y/\mu_y})^2 + (\frac{\mu_x}{\mu_y} - 1)^2} \quad (5)$$

where r is the Pearson correlation coefficient between the predictions (x) and observations (y) , μ_x and μ_y are the mean values of the predictions and observations, respectively; and σ_x and σ_y represent the standard deviations of the predictions and observations.

3. Result and Discussion

3.1. Preprocessing dan interpolasi temporal.

The preprocessing and temporal regularization processes were conducted to ensure the consistency of observation time intervals in the Persistent Scatterer Interferometric Synthetic Aperture Radar (PS-InSAR) data. This dataset served as the foundation for analyzing ground surface deformation in the DKI Jakarta area. The preprocessing stage included data duplication removal, handling of missing values, and outlier detection. After the cleaning stage was completed, temporal regularization was applied so that all observation points had a uniform time interval of 11 days, consistent with the revisit period of the Sentinel-1A satellite. The cleaned dataset consisted of 91,987 observation points, covering the period from January 2017 to December 2021. Before regularization, the deformation time series exhibited irregular observation intervals, with 29 observation dates varying between 11 and 88 days. This irregularity could potentially cause gradient imbalance during the learning process of time-series models such as LSTM.

After applying linear-based temporal interpolation with a fixed interval of $\Delta t = 11$ days, the number of observation timestamps increased to 122. This adjustment made the data more homogeneous and temporally continuous, allowing deformation patterns to be tracked more smoothly and consistently across observation periods. The comparison between deformation patterns before and after temporal regularization is illustrated in Figure 3.

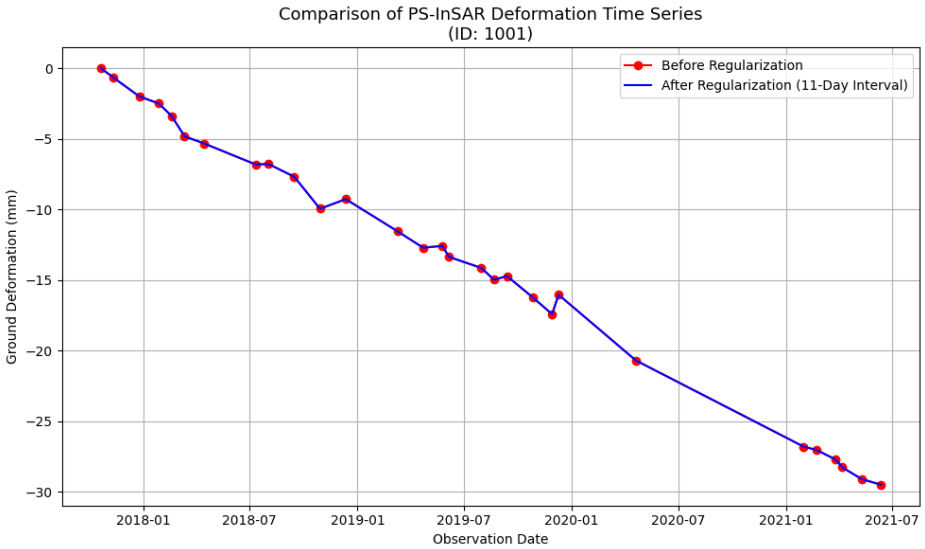

Figure 3. Comparison of PS-InSAR deformation time series before and after temporal regularization (fixed 11-day interval).

As shown in Figure 3, the data before regularization (red line) exhibit irregular intervals between acquisition dates, with several inconsistent temporal gaps. After applying temporal regularization (blue line), the cumulative deformation appears smoother and more continuous while following the same subsidence trend. These results indicate that the interpolation process successfully preserved the overall deformation trend without introducing value distortion, while also improving the temporal stability of the dataset. To evaluate the consistency and temporal correlation between variables after regularization, a Pearson correlation matrix analysis was performed. The results of this analysis are presented in Figure 4.

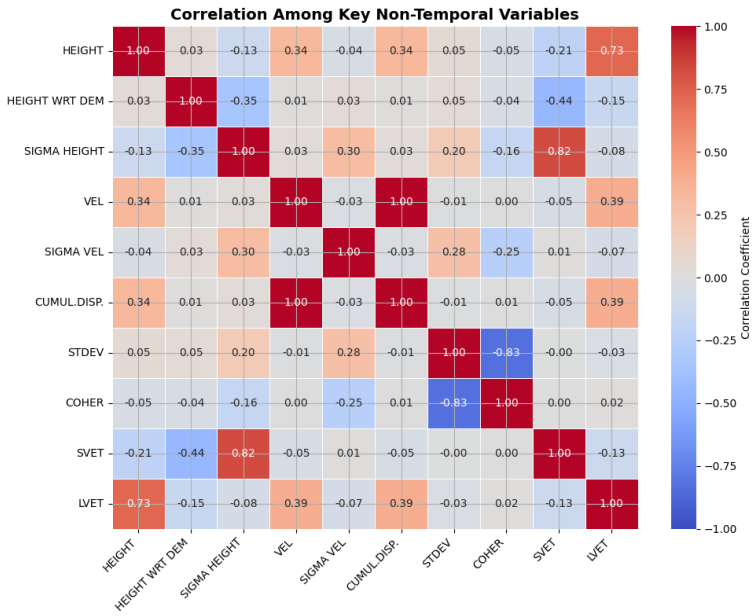

Figure 4. Correlation heatmap of the main non-temporal variables from the PS-InSAR dataset.

Correlation analysis was conducted to understand the relationships among variables derived from PS-InSAR processing before being used in the time-series modeling with LSTM. The correlation was calculated using the Pearson correlation coefficient (r) to assess the strength of linear relationships between non-temporal variable pairs, such as HEIGHT, VEL, COHER, and CUMUL.DISP. The correlation coefficient ranges from −1 to +1, where values approaching +1 indicate a strong positive relationship, while values near −1 indicate a strong negative relationship. Figure X presents the correlation matrix among the main non-temporal variables.

In general, the correlation patterns show significant linear relationships among several variable pairs directly associated with ground deformation dynamics. The VEL (Velocity) variable exhibits a strong positive correlation with CUMUL.DISP (Cumulative Displacement), with r≈0.99r \approx 0.99r≈0.99, indicating that an increase in deformation velocity corresponds directly to a greater cumulative displacement during the observation period. This correlation reinforces that deformation velocity is a major driving factor behind the total vertical displacement detected by radar. Meanwhile, a high correlation was also observed between SIGMA HEIGHT and SVET (r=0.82r = 0.82r=0.82), suggesting that variations in height uncertainty are closely related to the spatial distribution of phase velocity in the observation area. The negative correlation between COHER and STDEV (r=−0.83r = −0.83r=−0.83) indicates that higher coherence values correspond to smaller standard deviation values of deformation, reflecting good radar signal stability at those observation points.

Conversely, variables such as HEIGHT WRT DEM and SIGMA VEL showed low correlations with other parameters (< 0.3), implying that their contributions are more supplementary in explaining spatial variability rather than temporal dynamics.

These findings suggest that most non-temporal variables are complementary rather than redundant, allowing subsequent regularization and modeling processes to incorporate combinations of these variables without a high risk of multicollinearity. Overall, the correlation results confirm that VEL, CUMUL.DISP, and COHER are the key variables most representative of ground surface deformation within the study area. The positive and negative inter-variable relationships also indicate strong radar signal stability and adequate PS-InSAR data quality for use in LSTM model training.

3.2. LSTM model training results.

The Long Short-Term Memory (LSTM) model was trained using the PS-InSAR deformation data that had undergone temporal regularization with a fixed 11-day interval. The training aimed to learn the temporal relationships of ground surface deformation and generate continuous predictions of cumulative deformation. The dataset was chronologically divided into 80% for training and 20% for testing to prevent data leakage. This time-based split ensured that the model learned only from past data to predict future deformation. Each sequence window consisted of 12 consecutive time steps (132 days) used to predict the deformation value at the next time step.

Training was conducted for a maximum of 80 epochs with a batch size of 128. The Smooth L1 Loss (Huber Loss) function was employed to balance sensitivity to outliers while maintaining numerical stability. Optimization was performed using the Adam optimizer with an initial learning rate of 0.0005 and a weight decay of 1e-5. A learning rate scheduler was applied to automatically reduce the learning rate when the validation loss failed to improve for five consecutive epochs, while early stopping was implemented with a patience of 15 epochs.

Based on the training results, early stopping was triggered at epoch 42, when no significant improvement in validation loss was observed. The training loss decreased consistently from 0.00053 to 0.00021, while the validation loss fluctuated within the range of 0.0004–0.0006, showing a downward trend toward the end of training. This trend indicates that the model achieved a proper balance between learning and generalization, with no signs of overfitting.

Overall, the final evaluation results demonstrated that the LSTM model achieved excellent predictive performance. The values of $R^2 = 1.000$, RMSE = 0.322, and KGE = 0.9980 indicate that the model successfully captured temporal relationships with high accuracy and strong prediction stability. The model's performance was compared with that of Hidayah et al. [7], who utilized a Random Forest algorithm. Based on the final tuning results from that study (see Table 4), the LSTM model exhibited a notable performance improvement, particularly in temporal stability and generalization capability. The LSTM RMSE (0.322) was lower than that of the Random Forest model after tuning (0.3314), and its KGE (0.9980) was slightly higher than the previous model (0.9986). Although the numerical improvement appears minor, the temporal stability achieved by the LSTM model was significantly better, as it can capture sequential time dependencies that ensemble-based models such as Random Forest cannot effectively learn.

Based on Table 5, the LSTM model demonstrates performance that is comparable to, and slightly better than, the Random Forest model after parameter tuning. The main advantage of the LSTM lies in its ability to preserve sequential temporal patterns and capture nonlinear relationships across time steps, which cannot be effectively handled by ensemble-based approaches. This makes the LSTM model more suitable for analyzing time-series–based ground deformation data derived from PS-InSAR observations.

Table 5. Comparison of LSTM and random forest model performance.

Metric	**Random Forest** [7]	LSTM	Interpretation
R^2	0.9995	1.000	The LSTM model explains nearly all the variance in the temporal deformation data with higher precision.
MSE	0.1098	0.104	The slightly lower mean squared error of the LSTM model indicates better predictive accuracy.
RMSE	0.3314	0.322	A lower RMSE value suggests smaller differences between predicted and observed deformation values.
KGE	0.9986	0.9980	Both models exhibit excellent stability, but the LSTM shows more consistent temporal stability over long time sequences.

3.3. Spatial analysis of ground surface deformation.

Spatial analysis was conducted to illustrate the distribution of ground surface deformation in North Jakarta, based on the modeling results of the Long Short-Term Memory (LSTM) network applied to PS-InSAR data that had been temporally regularized at a fixed 11-day interval. The visualization of the mapping results is presented in Figure 2, which shows the distribution of deformation observation points during the 2017–2021 period. In general, the spatial pattern indicates that the northern coastal areas of Jakarta, particularly Tanjung Priok, Cilincing, and Pantai Indah Kapuk, experienced the most significant land subsidence. Based on the cumulative deformation values produced by the model, these areas exhibited subsidence exceeding −30 mm throughout the observation period. This phenomenon is consistent with previous studies linking significant subsidence in coastal zones to intensive urbanization, excessive groundwater extraction, and weak geotechnical conditions. In contrast, areas located further south, such as central Sunter and Kemayoran, displayed more stable deformation values, with average subsidence below −10 mm. This relative stability is likely influenced by denser soil composition and lower structural loading in these regions. The pattern demonstrates a north south deformation gradient, where subsidence rates tend to increase toward the coastline.

The LSTM model effectively represented this spatial variation, producing smoother and more continuous deformation maps compared to ensemble learning–based approaches such as Random Forest. With uniform temporal intervals, the model successfully reduced spatial fluctuations caused by irregular acquisition times in the raw PS-InSAR data. Furthermore, the distribution of predicted deformation points shows that areas with higher subsidence rates (red points) are densely concentrated along the coastline, while blue-dominated regions in central and southern North Jakarta indicate relatively stable ground conditions. Overall, these results reinforce the finding that North Jakarta remains an active subsidence zone, with a continuing downward trend through 2021. The combination of temporal regularization and the LSTM

model proved effective in capturing long-term and complex deformation patterns, while also improving the spatial consistency of the ground deformation mapping results.

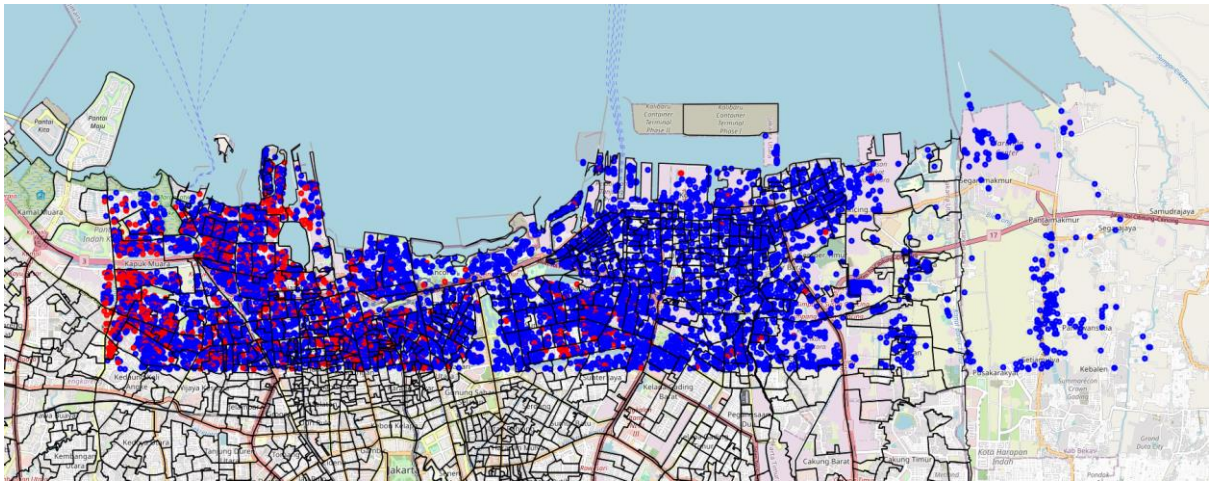

Figure 5. Spatial distribution of cumulative ground deformation in North Jakarta from 2017 to 2021 based on LSTM model prediction. Red areas indicate significant subsidence exceeding −30 mm, while blue areas represent stable zones with deformation less than −10 mm.

Despite the strong performance achieved by the proposed LSTM model, several limitations should be acknowledged to provide a balanced interpretation of the results. The use of a fixed 11-day temporal interpolation may introduce mild smoothing effects, potentially reducing the model's sensitivity to short-term deformation anomalies that occur between satellite acquisitions. In addition, because the model was trained exclusively on deformation characteristics unique to DKI Jakarta where subsidence is driven largely by groundwater extraction and coastal sediment compaction its generalisation to regions with different geological or anthropogenic conditions remains uncertain. The exceptionally high evaluation metrics may also reflect the high regularity of the interpolated time series, suggesting that future work should explore model robustness under noisier or irregular temporal inputs. Addressing these aspects through alternative interpolation methods, cross-regional testing, or the inclusion of additional environmental variables would further strengthen the applicability of the framework.

4. Conclusions

This study successfully developed a temporal analysis model of land subsidence in DKI Jakarta using a Long Short-Term Memory (LSTM) approach based on PS-InSAR data from the 2017–2021 period. Through the application of temporal regularization with a fixed 11-day interval, the deformation data became more consistent and homogeneous for time-series modeling. The LSTM model, consisting of three hidden layers, demonstrated excellent performance with values of R^2 = 1.000, MSE = 0.1098 mm, RMSE = 0.3314 mm, and KGE = 0.998, indicating that the predicted results were nearly identical to the actual observations. Compared to previous studies that employed the Random Forest algorithm, the LSTM model produced more temporally valid results by maintaining the chronological order of the data and avoiding data leakage. Spatially, the northern part of Jakarta particularly Cengkareng, Tanjung Priok, and Pantai Indah Kapuk, exhibited significant land subsidence exceeding −30 mm, while the southern areas, such as Jagakarsa and Kebayoran Baru, remained relatively stable with

subsidence below −5 mm. These findings are consistent with the geotechnical characteristics and urbanization pressure observed in the coastal regions. Overall, the LSTM-based PS-InSAR model effectively represented ground deformation patterns with high accuracy and stability, both temporally and spatially. The results of this research provide a scientific foundation for the development of AI-based subsidence monitoring systems and support risk mitigation efforts for land subsidence in high-risk urban areas such as DKI Jakarta. Beyond its scientific contribution, the findings of this study hold significant relevance for the development of Green Intelligent Systems in urban environmental management. Accurate deformation forecasting enables automated early-warning mechanisms, supports sustainable groundwater extraction policies, and improves the resilience of critical infrastructure in coastal megacities. By integrating PS-InSAR observations with deep learning–based temporal modeling, this research contributes to intelligent, environmentally aware monitoring systems that enhance climate adaptation strategies and promote sustainable land and water resource governance in DKI Jakarta.

Acknowledgments

The author sincerely expresses gratitude to the Geospatial Information Agency (BIG), the National Institute of Aeronautics and Space (LAPAN), and the Meteorology, Climatology, and Geophysics Agency (BMKG) of Indonesia for providing access to PS-InSAR Sentinel-1A data used in this study. The author also thanks the Ministry of Energy and Mineral Resources (ESDM) for supporting the availability of complementary environmental and groundwater data relevant to the analysis. Special appreciation is extended to the Department of Geodesy Engineering, Universitas Nasional, for academic guidance, facilities, and computational resources provided throughout this research. The author gratefully acknowledges the supervision, advice, and encouragement from academic mentors and reviewers who contributed valuable insights during the development of this paper. Finally, the author wishes to thank family members and close colleagues for their continuous moral support, motivation, and understanding during the completion of this study.

Competing Interest

The authors declare that they have no competing interests.

Author Contribution

Heni Fitriany: Conceptualization, Methodology, Data Collection, Data Analysis, Writing Original Draft Preparation, Visualization; Yasuhito Nagase: Supervision, Validation. Panca Dewi Pamungkasari: Supervision; Yunan Fauzi Wijaya: Supervision; Joko Widodo: Supervision; Muhammad Fauzan Azhiman: Writing.

Data Availability

The data supporting the findings of this study are available upon reasonable request.

References

[1] Bott, L.M.; Schöne, T.; Illigner, J.; Haghshenas Haghighi, M.; Gisevius, K.; Braun, B. (2021). Land subsidence in Jakarta and Semarang Bay – The relationship between physical processes, risk

perception, and household adaptation. *Ocean & Coastal Management*, *211*, 105775. https://doi.org/10.1016/j.ocecoaman.2021.105775.

[2] Sarah, D. (2022). Land subsidence hazard in Indonesia: Present research and challenges ahead. *Riset Geologi dan Pertambangan*, *32*(2), 83–100. https://doi.org/10.14203/risetgeotam2022.v32.1195.

[3] Abidin, H.Z.; Andreas, H.; Gumilar, I.; Brinkman, J.J. (2015). Study on the risk and impacts of land subsidence in Jakarta. In *Proceedings of the International Association of Hydrological Sciences*; Copernicus GmbH, 115–120. https://doi.org/10.5194/piahs-372-115-2015.

[4] Sidiq, T.P.; Gumilar, I.; Abidin, H.Z.; Meilano, I.; Purwarianti, A.; Lestari, R. (2025). Spatial distribution and monitoring of land subsidence using Sentinel-1 SAR data in Java, Indonesia. *Applied Sciences (Switzerland)*, *15*(7), 3732. https://doi.org/10.3390/app15073732.

[5] Widodo, J.; Trihatmoko, E.; Setyaningrum, N.; Izumi, Y.; Handika, R.; Ardha, M.; Arief, R.; Sobue, S.; Nurlinda, N.; Pranantya, P.A.; et al. (2025). Technical and policy analysis: Time series of land subsidence for the evaluation of the Jakarta groundwater-free zone. *Urban Science*, *9*(3), 67. https://doi.org/10.3390/urbansci9030067.

[6] Hakim, W.L.; Achmad, A.R.; Lee, C.W. (2020). Land subsidence susceptibility mapping in Jakarta using functional and meta-ensemble machine learning algorithm based on time-series InSAR data. *Remote Sensing (Basel)*, *12*(21), 3627. https://doi.org/10.3390/rs12213627.

[7] Hidayah, C.N.; Pamungkasari, P.D.; Ningsih, S.; Azhiman, M.F.; Widodo, J.; Widayaka, E.S. (2025). Land subsidence analysis using machine learning algorithm Random Forest method in DKI Jakarta. *Green Intelligent Systems and Applications*, *5*(1), 106–122. https://doi.org/10.53623/gisa.v5i1.606.

[8] Li, H.; Zhu, L.; Gong, H.; Sun, H.; Yu, J. (2020). Land subsidence modelling using a long short-term memory algorithm based on time-series datasets. In *Proceedings of the International Association of Hydrological Sciences*; Copernicus GmbH, 505–510. https://doi.org/10.5194/piahs-382-505-2020.

[9] Liu, Y.; Zhang, J. (2023). Integrating SBAS-InSAR and AT-LSTM for time-series analysis and prediction method of ground subsidence in mining areas. *Remote Sensing (Basel)*, *15*(13), 3409. https://doi.org/10.3390/rs15133409.

[10] Zhu, X.X.; Bamler, R. (2014). Superresolving SAR tomography for multidimensional imaging of urban areas: Compressive sensing-based TomoSAR inversion. *IEEE Signal Processing Magazine*, *31*(4), 51–58. https://doi.org/10.1109/MSP.2014.2312098.

[11] Morishita, Y.; Lazecky, M.; Wright, T.J.; Weiss, J.R.; Elliott, J.R.; Hooper, A. (2020). LiCSBAS: An open-source InSAR time series analysis package integrated with the LiCSAR automated Sentinel-1 InSAR processor. *Remote Sensing (Basel)*, *12*(3), 424. https://doi.org/10.3390/rs12030424.

[12] Soni, R.; Alam, M.S.; Vishwakarma, G.K. (2025). Prediction of InSAR deformation time-series using improved LSTM deep learning model. *Scientific Reports*, *15*, 5333. https://doi.org/10.1038/s41598-024-83084-1.